POLITECNICO DI TORINO
Repository ISTITUZIONALE

Assessing Reactive Responses and Gathering Restrictions for Eradicating Epidemic Diseases on Networks with Higher-Order Interactions

Original
Assessing Reactive Responses and Gathering Restrictions for Eradicating Epidemic Diseases on Networks with Higher-Order Interactions / Zino, L., Rizzo, A.. - In: IEEE TRANSACTIONS ON CONTROL OF NETWORK SYSTEMS. - ISSN 2325-5870. - ELETTRONICO. - 13:1(2026), pp. 277-287. [10.1109/tcns.2025.3629505]

Availability:
This version is available at: 11583/3004934 since: 2025-11-07T04:02:45Z

Publisher:
IEEE

Published
DOI:10.1109/tcns.2025.3629505

Terms of use:

This article is made available under terms and conditions as specified in the corresponding bibliographic description in the repository

Publisher copyright
IEEE postprint/Author's Accepted Manuscript

©2026 IEEE. Personal use of this material is permitted. Permission from IEEE must be obtained for all other uses, in any current or future media, including reprinting/republishing this material for advertising or promotional purposes, creating new collecting works, for resale or lists, or reuse of any copyrighted component of this work in other works.

(Article begins on next page)

19 November 2026

Assessing Reactive Responses and Gathering Restrictions for Eradicating Epidemic Diseases on Networks with Higher-Order Interactions

Lorenzo Zino, *Senior Member, IEEE* and Alessandro Rizzo, *Senior Member, IEEE*

***Abstract*— We characterize the dynamics of epidemic disease propagation on realistic temporal networks, where individuals participate in both pairwise and higher-order interactions. The latter captures large gatherings that may lead to superspreading events. We introduce an analytically tractable mathematical model for these temporal networks, based on continuous-time activity-driven networks, and study a susceptible–infected–susceptible (SIS) model spreading on its fabric. Utilizing a mean-field approach, we derive a system of ordinary differential equations (ODEs) that dictate the mean dynamics of the SIS process. By analyzing these ODEs, we identify the epidemic threshold of the model—revealing a phase transition between a regime where trajectories converge to a disease-free equilibrium and one where they stabilize at an endemic equilibrium (EE)—and delineate the unique EE for homogeneous networks. Subsequently, we integrate two distinct control measures into the model: i) restricting gatherings and ii) promoting a reactive behavioral response. We evaluate the efficacy of these control measures by computing the epidemic threshold of the controlled SIS model and employing various tools, including sensitivity analysis, mathematical optimization, and numerical simulations, to quantitatively assess how the control measures elevate the threshold, thus aiding in disease eradication, and how to amalgamate them for designing an optimal control policy.**

***Index Terms*— Complex networks, differential equations, epidemics, higher-order, Markov process, optimization**

I. Introduction

Mathematical models of epidemic propagation on temporal networks have garnered significant interest across various scientific domains due to their capability to represent the continuously changing contact patterns between individuals, which often facilitate the transmission of infectious diseases [1]–[6]. During the COVID-19 pandemic, it became evident within the scientific community that large gatherings substantially contribute to the spread of contagion, resulting in *superspreading events* [7]–[10], where infection spreads much more than usual. However, traditional epidemic models on temporal networks, which primarily focus on pairwise interactions between individuals, are inadequate to represent events that involve multiple participants, highlighting the necessity for the advancement of novel mathematical frameworks.

The authors are with the Department of Electronics and Telecommunications, Politecnico di Torino, Torino, Italy (e-mail: {lorenzo.zino, alessandro rizzo}@polito.it).

Higher-order networks have recently emerged as an effective approach to represent group interactions [11]–[14]. However, their mathematical complexity often hinders the analytical tractability of epidemic models spreading on top of them. In fact, existing results are mainly based on Monte Carlo numerical simulations [14]–[17], while rigorous analytical results are often limited to static higher-order networks [18]–[20]. This work builds on our previous effort [21] proposing a novel analytically-tractable paradigm for real-world temporal networks that advances the existing literature by incorporating both pairwise and higher-order interactions in a realistic and parsimonious model, which is then used to develop a new framework to assess and optimize intervention policies.

The formulation of accurate mathematical models for the propagation of epidemics provides potent instruments for assisting public health authorities in times of health crisis. Specifically, the integration of these models with methodologies derived from control theory and optimization has facilitated the derivation of model-informed tools to manage various aspects of an epidemic outbreak using control-theoretic approaches (see, e.g. [22], [23]), such as optimal drug distribution [24]–[28], strategic planning of vaccination campaigns [29]–[31], and the guidance of collective behavioral responses [32]–[34]. Certain approaches have proven to be effective during the COVID-19 health crisis [35]–[39]. However, the performance of these tools depends on the presence of precise and analytically tractable models. Consequently, the absence of such models for temporal networks with higher-order interactions has constrained the capacity to develop mathematically principled methodologies for examining the impact of gatherings during an epidemic outbreak and evaluating the effectiveness of policies predicated on their restriction.

In this paper, we fill in this gap by introducing an innovative framework for temporal networks encompassing both pairwise and higher-order interactions. This framework is grounded in the continuous-time formulation of activity-driven networks (ADNs) [40], wherein each individual forms temporal interactions—either pairwise or involving multiple individuals) in a stochastic fashion, individuals—stochastically, based on their (often heterogeneous) social activity levels. Subsequently, we examine a susceptible-infected-susceptible (SIS) epidemic model propagating atop the temporal network [5], which is an established proxy for many diseases that provides negligible natural immunity, such as common cold or many sexually

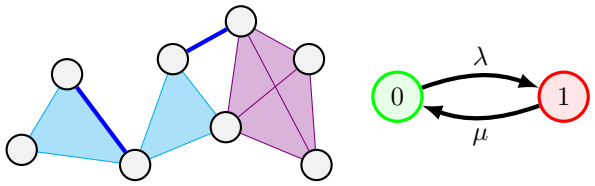
transmitted diseases [41].

After deriving the exact dynamics of the Markov process that governs the SIS epidemic spreading, we use a mean-field approach to obtain a system of coupled nonlinear ordinary differential equations (ODEs) that approximates the emergent behavior of the epidemics in the limit of large networks [42]. By examining this system of ODEs, we delineate a phase transition between two distinct regimes: when the infection rate falls below a certain threshold *epidemic threshold*, which is derived explicitly, the disease-free equilibrium (DFE) demonstrates global asymptotic stability, signifying prompt eradication of the epidemic outbreak. Conversely, if the infection rate exceeds this threshold, the DFE becomes unstable, resulting in trajectories that converge to one or more endemic equilibria (EE). Interestingly, our results show that higher-order interactions can critically favor the spread of a disease, supporting the ban of large gatherings during an epidemic outbreak, which has been implemented, e.g., during the COVID-19 health crisis [43].

Two strategies for taming the spread of the epidemic are devised and implemented through two different control actions encapsulated in the model: i) implementing gathering restrictions and ii) eliciting a reactive behavioral response, inspired by [44]. By employing the mean-field approach once more [42], we derive a system of ordinary differential equations (ODEs) whose analysis enables a quantitative assessment of the effectiveness of the two control actions in eradicating the epidemic disease. Notably, our analysis reveals that, within homogeneous networks, imposing restrictions on gatherings is consistently more effective. Conversely, in scenarios characterized by heterogeneity within the population, determining the most effective control action becomes inherently complex due to the presence of highly active individuals who may function as superspreaders. To address this complexity, we formulate an optimization problem that serves as the basis for developing optimal control policies through the two control strategies.

Some of the results presented in this paper have appeared, in a preliminary form, in [21]. Here, we fundamentally generalize and strengthen our effort in several directions. While the model proposed in [21] only included higher-order interactions, here we extend the model to capture the coexistence of both pairwise and higher-order interactions, which are typical of real-world networks. The analysis of the SIS epidemic model performed in this extended setting leads to a new formulation for the epidemic threshold (Theorem 1). Additionally, new results on homogeneous networks, including the characterization of the EE are established (Corollary 1), offering new analytical insights into epidemic processes. Finally, building on this generalization, we are able to use gathering restrictions as a control lever for disease eradication. In particular, after exploring its effectiveness (as rigorously established in Theorem 2), we use our results to design optimal control policies.

The remainder of the paper is organized as follows. In Section II, we introduce the uncontrolled model, whose dynamics is derived in Section III, and studied in Section IV. In Section V, we incorporate the control actions, whose effectiveness is then studied in Section VI. Section VII concludes the paper.



(a) Higher-order network (b) SIS model

Fig. 1: (a) a network with simplicial complexes of order $m = 1$ (pairwise interactions) in blue, of order $m = 2$ in cyan, and of order $m = 3$ in violet. (b) schematic of the transitions of an SIS model.

II. Model

A. Notation and mathematical preliminaries

The real, real nonnegative, strictly positive real, and strictly positive integer numbers are denoted by $\mathbb{R}$, $\mathbb{R}_{\geq 0}$, $\mathbb{R}_{>0}$, and $\mathbb{Z}_{>0}$, respectively. Given a function $x(t)$, we denote $x(t^-) := \lim_{s \nearrow t} x(s)$ and $x(t^+) := \lim_{s \searrow t} x(s)$. Given an event E, we denote by $\mathbb{P}[E]$ the probability that E occurs. Given a random variable X, we denote its expected value by $\mathbb{E}[X]$. Finally, we summarize the following definitions and properties related to stochastic processes.

Definition 1 (Poisson clock)**.** *A (homogeneous) Poisson clock with rate $\rho \in \mathbb{R}_{\geq 0}$ is a continuous-time stochastic process, represented by its counting process $N(t) \in \mathbb{Z}_{\geq 0}$, which satisfies*

$$\mathbb{P}[N(t + \Delta t) - N(t) = 1] = \rho \Delta t + o(\Delta t)\,, \tag{1}$$

for any $\Delta t \in \mathbb{R}_{>0}$, where the Landau little-o notation $o(\Delta t)$ is associated with the limit $\Delta t \searrow 0$. If $N(t)$ has an increment at time $t \in \mathbb{R}_{\geq 0}$, we say that the clock ticks at time t.

Proposition 1 ([45])**.** *The following properties hold true:*

i) *Let E be an event triggered by the first tick of any clock of a set of independent Poisson clocks with rates $\rho_1, \ldots, \rho_\ell$. Then, E can be equivalently described as triggered by a Poisson clock with rate equal to the sum $\sum_{h=1}^{\ell} \rho_h$;*

ii) *Let E be an event that occurs with probability $q \in [0, 1]$ if a Poisson clock with rate of ρ ticks. Then, E can be equivalently described as triggered by a Poisson clock with a rate equal to the product $q\,\rho$.*

Definition 2 (Markov process)**.** *A (homogeneous) Markov process is a continuous-time stochastic process $X(t)$ whose transitions are triggered by independent Poisson clocks. Specifically, for any pair of states a, b belonging to a state space $\mathcal{X}$, $X(t)$ has a transition from a to b if a Poisson clock with rate q^{ab} ticks, i.e.*

$$\mathbb{P}[X(t + \Delta t) = b | X(t) = a] = q^{ab} \Delta t + o(\Delta t)\,. \tag{2}$$

The matrix Q that gathers all the Poisson clocks' rates is termed transition rate matrix.

B. Continuous-time higher-order ADNs

Higher-order networks can be described using simplicial complexes, which are defined as follows.

Definition 3 (Simplicial Complex)**.** *Given a network with node set $\mathcal{V}$, a simplicial complex of order $m \in \mathbb{Z}_{>0}$ is a set of*

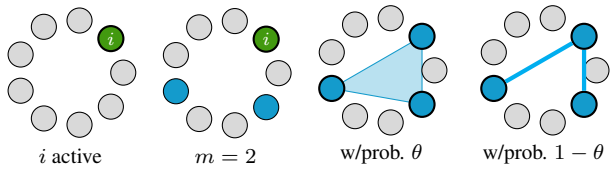


Fig. 2: Schematic of the temporal network formation process.

TABLE I: Model variables and parameters.

n	population of the network
$x_i(t)$	health state of individual i at time t
a_i	activity rate of individual i
m	number of interactions established by active individuals
θ	tendency to engage in higher-order interactions
λ	infection rate
μ	recovery rate

$m+1$ *nodes* $\kappa = \{v_1, \dots, v_{m+1}\} \subset \mathcal{V}$*, with* $v_i \neq v_j$*, for all* $i, j \in \{1, \dots, m+1\}$.

In other words, a simplicial complex of order m represents an interaction that involves $m+1$ distinct nodes, as illustrated in Fig. 1a. For $m = 1$, the corresponding simplicial complex is formed by a pair of nodes, that is, a link.

We consider a population of $n \in \mathbb{Z}_{>0}$ individuals, $\mathcal{V} = \{1, \dots, n\}$, each associated with a node in an undirected higher-order temporal network $(\mathcal{V}, \mathcal{K}(t)), \in \mathbb{R}_{\geq 0}$, with the set $\mathcal{K}(t)$ containing all simplicial complexes connecting nodes at time t. Individuals can engage in pairwise or higher-order interactions. Specifically, we introduce a parameter $\theta \in [0, 1]$ that represents the tendency of the population to engage in higher-order interactions, favoring the occurrence of super-spreading events.

To generate such a temporal network, we build on the theory of continuous-time ADNs [40], extending the paradigm developed in [21] to higher-order interactions. Specifically, each individual is characterized by an activity rate $a_i \in \mathbb{R}_{>0}$, which captures the individual's tendency to initiate social interactions and by a common constant parameter $m \in \mathbb{Z}_{>0}$, which captures the order of the interaction in case of a higher-order interaction. The network formation process (illustrated in Fig. 2), is detailed in the following:

1) At time $t = 0$, we initialize $\mathcal{K}(t) = \emptyset$. Each node $i \in \mathcal{V}$ is associated with a Poisson clock with rate equal to a_i, each independent of the others;
2) Time progresses until any of the Poisson clocks ticks;
3) When the clock associated with $i \in \mathcal{V}$ ticks at time t, individual i is said to be *active*;
4) The active individual i selects a m-uple of fellow individuals $j_1, \dots j_m$, uniformly at random among all possible m-uples of individuals. Then:
   a) With probability $\theta \in [0, 1]$, i engages in a higher-order interaction with these individuals: The order-m simplicial complex $\kappa = \{i, j_1, \dots, j_m\}$ is added to $\mathcal{K}(t)$;
   b) Otherwise, with probability $1 - \theta$, i engages in a pairwise interaction with these individuals: The m order-1 simplicial complexes (i.e., standard links) $\kappa_1, \dots, \kappa_m$ are added to $\mathcal{K}(t)$, with $\kappa_\ell = \{i, j_\ell\}$;
5) The simplicial complexes generated at time t are immediately removed from the set, the Poisson process associated with node i is reinitialized, and the process is resumed from item 2).

Remark 1. *If* $\theta = 0$*, this algorithm reduces to the one of a standard continuous-time ADN [40]; on the other hand, if* $\theta = 1$*, it reduces to the higher-order ADNs proposed in [21].*

The parsimoniousness of this network formation model, where the tendency to engage in higher-order interactions is captured by a single parameter θ, is advantageous for several reasons. From the theoretical point of view, this yields analytically tractability, whereby the impact of θ can be evaluated without other confounding factors, as we shall see in the following. From the practical point of view, a single parameter θ can be reliably estimated from real-world data on social contacts, e.g., large-scale surveys [46].

C. Susceptible–infected–susceptible model

We study an SIS epidemic process that spreads on top of the temporal network defined in the previous section. According this model, the health state of each individual $i \in \mathcal{V}$ is characterized by a binary variable

$$x_i(t) = \begin{cases} 0 & \text{if } i \text{ is susceptible at time } t, \\ 1 & \text{if } i \text{ is infected at time } t. \end{cases} \tag{3}$$

States are gathered into the vector $\boldsymbol{x}(t) = [x_1(t) \dots x_n(t)]^\top$, which is the state variable of the network.

Two contrasting mechanisms determine the evolution of the health state. First, if a susceptible individual i ($x_i(t^-) = 0$) interacts with an infected individual at time t (i.e., if $\exists\, \kappa \in \mathcal{K}(t)$ with $i, j \in \kappa$ and $x_j(t) = 1$), then, with probability $\lambda \in [0, 1]$, *contagion* occurs and i becomes infected ($x_i(t^+) = 1$). Second, an infected individual j ($x_j(t^-) = 1$) spontaneously *recovers* according to a Poisson clock with rate $\mu \in \mathbb{R}_{>0}$. In the SIS model, it is assumed that recovered individuals are immediately susceptible again to the disease (i.e., $x_j(t^+) = 0$). All probabilistic mechanisms are independent of the others. The SIS process is illustrated in Fig. 1b, and all its variables and parameters are summarized in Table I.

III. Uncontrolled SIS Dynamics

A. Markov process

Both the network formation process and the SIS epidemic process are governed by independent Poisson processes. Hence, the state variable $x(t)$ evolves according to a set of independent Poisson clocks, ultimately yielding a Markov process (see Definition 2). Specifically, $x(t)$ is an n-dimensional continuous-time Markov process. To simplify the notation, we can use a block-level notation for matrix Q, and for each individual $i \in \mathcal{V}$ we write the probability that i switches their state in a time-interval of duration $\Delta t \in \mathbb{R}_{>0}$ as

$$\mathbb{P}[x_i(t + \Delta t) = b \,|\, x_i(t) = a] = q_i^{ab}(\boldsymbol{x}(t))\Delta t + o(\Delta t), \tag{4}$$

with $a, b \in \{0, 1\}$ and $b \neq a$. The entries of the transition rate matrix $q_i^{01}(\cdot)$ and $q_i^{10}(\cdot)$ are associated with the two

mechanisms of contagion and recovery, respectively, and their values, which may depend on time through the state of the system $x(t)$, are explicitly derived in the following.

Proposition 2. *The transition rates in* (4) *for the SIS model when* $\boldsymbol{x}(t) = \boldsymbol{x}$ *are equal to*

$$q_i^{01}(x) = \lambda a_i \frac{m}{n-1} \sum_{j \in \mathcal{V}} x_j + \lambda \frac{m}{n-1} \sum_{j \in \mathcal{V}} a_j x_j + \lambda\theta \frac{m(m-1)}{(n-1)(n-2)} \sum_{j \in \mathcal{V}} x_j \sum_{\ell \in \mathcal{V} \setminus \{i,j\}} a_\ell, \tag{5a}$$

and

$$q_i^{10}(x) = \mu. \tag{5b}$$

Proof. The proof is reported in Appendix A □

B. Mean-field equations

The complexity of the transition rates computed in Proposition 2, which are coupled and nonlinear, and the dimension of the state space $\{0,1\}^n$, which grows exponentially as $n \to \infty$, hinder the direct analytical tractability of the Markov process $x(t)$. We tackle this issue through a mean-field relaxation along the lines of [42], focusing on the mean dynamics of the health state of each individual $i \in \mathcal{V}$, i.e.,

$$y_i(t) := \mathbb{E}[x_i(t)] = \mathbb{P}[x_i(t) = 1], \tag{6}$$

which coincides with the probability for individual i to be infected. These variables are then gathered in the mean-field state variable $\boldsymbol{y}(t) = [y_1(t), \dots y_n(t)]$.

Following [42], the dynamics of the mean-field state variable is described by a system of n ordinary differential equations (ODEs), obtained by approximating the expected value of the transition rates with the transition rates for the mean dynamics, i.e., $\mathbb{E}[q_i^{01}(\boldsymbol{x}(t))] \approx q_i^{01}(\mathbb{E}[\boldsymbol{x}(t)]) = q_i^{01}(\boldsymbol{y}(t))$.

Proposition 3. *The mean-field dynamics of the SIS model is the solution of the following system of ODEs, for* $i \in \mathcal{V}$*:*

$$\dot{y}_i = (1-y_i)\lambda m \left[a_i \frac{1}{n-1} \sum_{j \in \mathcal{V}} y_j + \frac{1}{n-1} \sum_{j \in \mathcal{V}} a_j y_j + \theta \frac{m-1}{(n-1)(n-2)} \sum\nolimits_{j \in \mathcal{V}} y_j \sum\nolimits_{\ell \in \mathcal{V} \setminus \{i,j\}} a_\ell \right] - \mu y_i. \tag{7}$$

Proof. The result is obtained by starting from the general mean-filed dynamics: $\dot{y}_i = (1-y_i) q_i^{01}(\boldsymbol{y}) - y_i q_i^{10}(\boldsymbol{y})$ (see [21] for its derivation), and substituting the rates from (5). □

For large networks, in the limit $n \to \infty$, the epidemic prevalence[1] for the stochastic model $I(t) := \frac{1}{n}|\{i \in \mathcal{V} : x_i(t) = 1\}|$ can be approximated for any finite time-horizon within an arbitrary precision [42] as $I(t) \approx \frac{1}{n} \sum_{i \in \mathcal{V}} y_i(t)$ (see, e.g., [33] for a numerical comparison). Hence, for sufficiently large networks, we can study the behavior of the epidemics at the population level using the mean-field equations derived in (7). To facilitate such a study, we define a macroscopic variable representing the average probability for a generic node to be infected as

$$z_1(t) := \frac{1}{n} \sum\nolimits_{i \in \mathcal{V}} y_i(t), \tag{8}$$

which coincides with the approximation of the mean-field epidemic prevalence. Similarly, we define the first and second moment of the activity distribution as

$$\alpha_1 := \frac{1}{n} \sum\nolimits_{i \in \mathcal{V}} a_i, \qquad \alpha_2 := \frac{1}{n} \sum\nolimits_{i \in \mathcal{V}} i^2, \tag{9}$$

where α_1 captures the mean social activity of the population and α_2 the heterogeneity of its distribution. To have a clearer parametrization of the level of heterogeneity of a population, we define the coefficient of variation

$$c_v := \frac{\sqrt{\alpha_2}}{\alpha_1}, \tag{10}$$

which attains its minimum when the population is homogeneous (i.e., $c_v = 1$), and increases with the heterogeneity.

IV. Results for the Uncontrolled SIS Model

We start our analysis of the uncontrolled mean-field dynamics by proving that all its trajectories converge to an equilibrium.

Proposition 4. *Any trajectory of* (7) *converges to an equilibrium.*

Proof. First, we observe that the domain $\mathcal{D} = [0,1]^n$ is compact and convex and (7) is Lipschitz-continuous. Moreover, at the boundary $y_i = 0$, it holds $\dot{y}_i \geq 0$, since the last term of (7) is zero and the others are all nonnegative; at the boundary $y_i = 1$, it holds $\dot{y}_i = -\mu < 0$. Hence, Nagumo's Theorem [47] yields positive invariance. Then, we consider the Jacobian matrix of (7), whose generic off-diagonal entry is equal to

$$J_{ij} = (1-y_i)\frac{\lambda m}{n-1} \left(a_i + a_j + \theta \frac{m-1}{n-2} \sum_{\ell \neq i,j} a_\ell \right) \geq 0. \tag{11}$$

Consequently, (7) is a monotone dynamical system over the compact invariant domain $\mathcal{D}$, and all its trajectories necessarily converge to an equilibrium [48]. □

Proposition 4 guarantees that the mean-field dynamics always converges to an equilibrium. By further analyzing (7), we can provide a characterization of its possible equilibria.

Proposition 5. *The system in* (7) *always has the disease-free equilibrium (DFE)* $\hat{\boldsymbol{y}} = \boldsymbol{0}$*. Moreover, any other equilibrium is an endemic equilibrium (EE), with* $\hat{y}_i > 0$ *for all* $i \in \mathcal{V}$*.*

Proof. After verifying that the DFE is an equilibrium, we prove the second statement by contradiction. Assume there exists an equilibrium $\hat{\boldsymbol{y}} \neq \boldsymbol{0}$ and a node $i \in \mathcal{V}$ such that $\hat{y}_i = 0$. Then, being $\hat{\boldsymbol{y}} \neq \boldsymbol{0}$, there exists $j \in \mathcal{V}$ with $\hat{y}_j > 0$. From (7), we bound $\dot{y}_i \geq \frac{1}{n-1}\lambda m(a_i + a_j + \theta \frac{m-1}{n-2} \sum_{\ell \neq i,j} a_\ell)\hat{y}_i > 0$. Hence, $\hat{\boldsymbol{y}}$ is not an equilibrium, which leads to a contradiction, yielding the claim. □

Propositions 4 and 5 guarantee that the mean-field dynamics always converges either to the DFE or to an EE. In these

[1] In epidemiology, the epidemic prevalence is the proportion of a population that has a specific disease or condition at a specific time.

regards, a key concept in mathematical epidemic models is the *epidemic threshold*. Namely, the epidemic threshold σ is a function of the model parameters that characterizes a phase transition in the emergent behavior of the system. If the ratio between infection rate and recovery rate $\lambda/\mu < \sigma$, then the DFE is globally exponentially stable, implying that all trajectories will converge to it. Otherwise, the DFE is unstable and (almost) all trajectories converge to an EE. In other words, the epidemic threshold determines a critical value for the contagion rate such that, if the disease is sufficiently contagious, then it produces a long-lasting outbreak; otherwise, it is quickly eradicated. The analytical computation of such a threshold is thus a problem of paramount importance in mathematical epidemiology. Here, we compute such a threshold in the limit of large-scale networks $n \to \infty$, i.e., when the approximation $I(t) \approx z_1(t)$ holds true, and the mean-field equation is a good proxy for the Markov chain.

Theorem 1. *For large networks ($n \to \infty$), the epidemic threshold for the SIS dynamics in* (7) *is*

$$\sigma = \frac{2}{m\alpha_1[\theta m + 2 - \theta + \sqrt{\theta(m-1)(\theta m + 4 - \theta) + 4c_v^2}]}. \tag{12}$$

If $\frac{\lambda}{\mu} < \sigma$, then all trajectories converge to the DFE. If $\frac{\lambda}{\mu} > \sigma$, then all trajectories with initial conditions different from the DFE converge to an EE.

Proof. We start by studying the (local) stability of the DFE. We observe that $z_1 = 0 \iff \boldsymbol{y} = 0$. Hence, we can study the local stability of the DFE by studying the local stability of $z_1 = 0$. Following [33], we introduce an auxiliary variable

$$z_2 = \frac{1}{n}\sum\nolimits_{i\in\mathcal{V}} a_i y_i, \tag{13}$$

and we consider a planar system made by the two variables z_1 and z_2. Clearly, it still holds that the origins of (7) and of the planar system coincide, i.e., $(z_1, z_2) = (0, 0) \iff \boldsymbol{y} = 0$.

In the limit $n \to \infty$, we observe the following identities:

$$z_1 = \lim_{n\to\infty} \frac{1}{n-1}\sum_{i\in\mathcal{V}} y_i = \lim_{n\to\infty} \frac{1}{n}\sum_{i\in\mathcal{V}} y_i, \tag{14a}$$

$$z_2 = \lim_{n\to\infty} \frac{1}{n-1}\sum_{i\in\mathcal{V}} a_i y_i = \lim_{n\to\infty} \frac{1}{n}\sum_{i\in\mathcal{V}} a_i y_i, \tag{14b}$$

$$\alpha_1 = \lim_{n\to\infty} \frac{1}{n-2}\sum_{\ell\in\mathcal{V}\setminus\{i,j\}} a_\ell = \lim_{n\to\infty} \frac{1}{n}\sum_{\ell\in\mathcal{V}} a_\ell, \tag{14c}$$

where the latter holds for any $i, j \in \mathcal{V}$. Using (14), we write (7) as

$$\dot{y}_i = (1-y_i)\lambda m\Big[a_i z_1 + z_2 + \theta(m-1)\alpha_1 z_1\Big] - \mu y_i, \tag{15}$$

which we use to compute the dynamics for the planar system of interest (z_1, z_2), as

$$\begin{aligned}\dot{z}_1 = \frac{1}{n}\sum\nolimits_{i\in\mathcal{V}} \dot{y}_i = -\mu z_1 + \lambda m\Big[&\alpha_1 z_1 - z_1 z_2 \\ &+ z_2(1-z_1) + \theta(m-1)\alpha_1 z_1(1-z_1)\Big],\end{aligned} \tag{16a}$$

and

$$\begin{aligned}\dot{z}_2 = \frac{1}{n}\sum_{i\in\mathcal{V}} a_i\dot{y}_i = -\mu z_2 + \lambda m\Big[&\alpha_2 z_1 - z_1\frac{1}{n}\sum_{i\in\mathcal{V}} a_i^2 y_i \\ &+ z_2(\alpha_1 - z_2) + \theta(m-1)\alpha_1 z_1(\alpha_1 - z_2)\Big].\end{aligned} \tag{16b}$$

Then, we linearize (16) about the origin to study its local stability, obtaining

$$\begin{aligned}\dot{z}_1 &= -\mu z_1 + \lambda m(\theta m + 1 - \theta)\alpha_1 z_1 + \lambda m z_2 \\ \dot{z}_2 &= -\mu z_2 + \lambda m(\theta(m-1)\alpha_1^2 + \alpha_2) z_1 + \lambda m\alpha_1 z_2,\end{aligned} \tag{17}$$

we compute the Jacobian matrix of (17) and we evaluate it at the origin, obtaining

$$J_{0,0} = \begin{bmatrix} \lambda m(\theta m + 1 - \theta)\alpha_1 - \mu & \lambda m \\ \lambda m(\theta(m-1)\alpha_1^2 + \alpha_2) & \lambda m\alpha_1 - \mu \end{bmatrix}. \tag{18}$$

To compute its eigenvalues $\xi_{1,2}$, we define $\zeta_{1,2} = \xi_{1,2} + \mu$, and from (18), we obtain the characteristic polynomial

$$\zeta^2 - \lambda m(\theta m + 2 - \theta)\alpha_1\zeta - \lambda^2 m^2(\alpha_2 - \alpha_1^2), \tag{19}$$

from which we compute the two solutions for $\zeta_{1,2}$, as

$$\frac{\lambda m}{2}\Big[(\theta m + 2 - \theta)\alpha_1 \pm \sqrt{\theta(m-1)(\theta m + 4 - \theta)\alpha_1^2 + 4\alpha_2}\Big],$$

from which we obtain the two eigenvalues $\xi_{1,2} = \zeta_{1,2} - \mu$. The condition for local stability of the DFE is obtained by imposing negativity of the largest eigenvalue, which yields (12). Finally, local stability is extended to global stability along the lines of [21], by observing that the nonlinear terms in (15) are nonpositive and the system is monotonic (Proposition 4), which guarantees that the trajectory of the linearized system (which converges to the DFE) acts as an upper-bound on the trajectory of the nonlinear system, which necessarily converges to the DFE. In contrast, if the DFE is (locally) unstable, then the global convergence result in Proposition 5 guarantees convergence to an EE. □

Remark 2. *For $m = 1$, the threshold in* (12) *reduces to $\sigma = (\alpha_1 + \sqrt{\alpha_2})^{-1}$, as for the standard SIS model on ADNs [40], [49]. For $\theta = 1$, the threshold reduces to that of an SIS model on hADNs [21].*

Before incorporating control actions into the epidemic model, we would like to briefly discuss the analytical insights that Theorem 1 offers on the nontrivial impact of higher-order interactions on shaping the spread of epidemic diseases. The threshold σ should be interpreted as the maximal value of the ratio λ/μ that the network can handle without leading to an epidemic outbreak. In other words, larger values of the threshold are associated with networks in which diseases are easier to be eradicated. From (12), we observe that σ is monotonically decreasing in θ, which implies that higher-order interactions are always detrimental to the network resistance to epidemic spreading.

Some further insights can be gained by performing a comparison between the epidemic threshold in (12) and the one of a standard ADN, which is

$$\tilde{\sigma}_m = [M\alpha_1(1 + c_v)]^{-1}. \tag{20}$$

From a direct comparison between the two thresholds, we obtain

$$\frac{\sigma}{\tilde{\sigma}} = \frac{2+2c_v}{(\theta m+2-\theta)+\sqrt{\theta(m-1)(\theta m+4-\theta)+4c_v^2}}, \tag{21}$$

which is equal to 1 iff $m = 1$ or $\theta = 0$, or it is smaller than 1 otherwise —to make this claim, it is sufficient to check that (21) is monotonically decreasing in both m and θ. This implies that the epidemic threshold $\sigma < \tilde{\sigma}_m$, which means that it is always easier for a disease to spread in the presence of higher-order interactions, as illustrated in Fig. 3. This confirms empirical studies that indicate superspreading events as key drivers of an epidemic outbreak [7], [8]. Intuitively, such an effect increases with the tendency to engage in higher-order interactions θ and the order of the interaction m. Interestingly, the effect appears to be stronger for moderately heterogeneous networks. We believe that this is due to the fact that heterogeneity is another key driver of contagion [40], [49]. Hence, especially for moderate orders of interactions, heterogeneity might have a dominant role.

An interesting observation that emerges from Theorem 1 and (21) is that the presence of higher-order interactions is critical in the emergence of epidemic outbreak for diseases that would instead be below the threshold in a classical network of pairwise interactions only. A paradigmatic example comes from the 2022-23 mpox outbreak, which affected almost 100,000 individuals [50], despite its basic reproduction number is estimated to be smaller than 1, and thus no classical models would predict a global epidemic outbreak [51]. The presence of higher-order interactions, which has been empirically observed in correspondence of many mpox outbreaks [10], could instead decrease the threshold (as demonstrated by our analytical results), explaining the emergence of such outbreaks.

Finally, for homogeneous networks (formally stated in the following), we can provide a complete characterization of the emergent behavior of the system, by refining Theorem 1, proving the uniqueness of the EE, and providing a closed-form expression for it, as discussed in the following.

Assumption 1. *Assume that $a_i = \alpha_1$, for all $i \in \mathcal{V}$.*

Corollary 1. *Under Assumption 1, the epidemic threshold for the SIS dynamics in* (7) *reduces to*

$$\bar{\sigma} = \frac{1}{m\alpha_1(\theta m+2-\theta)}. \tag{22}$$

If $\frac{\lambda}{\mu} > \bar{\sigma}$, then any trajectories with initial conditions different from the DFE converges to the unique EE with

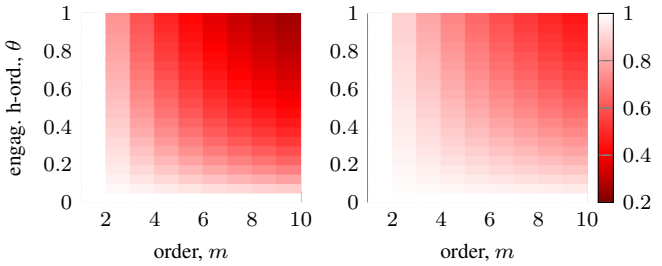
$$y_i = z_1 = 1 - \frac{\mu}{\lambda m\alpha_1(\theta m+2-\theta)}, \quad \forall i \in \mathcal{V}. \tag{23}$$

Proof. The threshold in (22) is immediately derived by posing $c_v = 1$ in (12). Then, being $a_i = \alpha_i$ for all $i \in \mathcal{V}$, it clearly holds that $z_2 = \frac{1}{n}\sum_{i\in\mathcal{V}} a_i y_i = \alpha_1 z_1$, which reduces (15) to

$$\dot{y}_i = (1-y_i)\lambda m 2\alpha_1 z_1(\theta m+2-\theta) - \mu y_i, \tag{24}$$

for all $i \in \mathcal{V}$, from which we derive

$$\dot{z}_1 = (1-z_1)z_1\lambda m\alpha_1(\theta m+2-\theta) - \mu z_1, \tag{25}$$



(a) $c_v = 1.5$ (b) $c_v = 4$

Fig. 3: Comparison between the epidemic threshold of an SIS model on a network with higher-order interactions and a standard ADN. The color intensity represents the ratio between the two thresholds $\sigma/\tilde{\sigma}$ for different levels of heterogeneity in the network, captured by the parameter c_v. The darker is the shade of red, the easier is for the disease to spread in the presence of higher-order interactions.

which has only two equilibria: the DFE $z_1 = 0$ and the EE in (23). Finally, from (24), we observe that $\dot{y}_i = 0$ iff $y_i = z_1$ at the EE, yielding the claim. □

Finally, it is worth noticing that the epidemic threshold in (1) has a continuous dependence on c_v. Hence results obtained in the homogeneous case can serve as reasonable approximations for mildly heterogeneous scenarios.

V. Controlled SIS Model

A. Model

We incorporate two control actions to help eradicate the epidemic disease, which are delineated in the following.

Gathering restrictions. We introduce a control parameter $u_1 \in [0,1]$, and we assume that the tendency to engage in higher-order interactions is function of u_1, i.e., $\theta = \theta(u_1)$. In the simplest scenario, we can assume a linear relation $\theta = 1-u_1$, where u_1 captures the effort placed in restricting large gatherings, which reduces the individuals' tendency to engage in higher-order interactions.

Behavioral response. We assume that infected individuals reduce their tendency to initiate social interactions by temporarily reducing their activity. To capture this phenomenon, we introduce a second control parameter $u_2 \in [0,1]$, which captures the stimulation of such a collective response. Inspired by [44], we assume that the activity of infected individuals is reduced by a fraction u_2. Hence, the effective activity of an individual becomes state-dependent, as

$$\hat{a}_i(x_i) = \begin{cases} a_i & \text{if } x_i = 0, \\ (1-u_2)a_i & \text{if } x_i = 1. \end{cases} \tag{26}$$

In summary, the two control parameters $u_1 \in [0,1]$ and $u_2 \in [0,1]$ capture the extent of effort exerted by public authorities in executing the respective control measures. It is important to mention that, before applying this model in real-world scenarios, one has first to understand how real-life actions (e.g., fines for attending large gatherings or enforcing quarantine to infected individuals) map into values of u_1 and u_2. In these regards, data on the COVID-19 crisis can

be extremely beneficial. In fact, different countries enacted different actions [52]. From these documented actions and using the corresponding infection time series and human mobility data (which are public available), one can evaluate the adherence to restrictions (estimating u_1), and calibrate the model to infer u_2.

Consequently, the main inquiry from the perspective of public health authorities is related to the formulation of an intervention strategy, defined by u_1 and u_2, with the objective of optimally mitigating an epidemic outbreak. To effectively address this inquiry, it is necessary to first derive and subsequently analyze the dynamics of the controlled SIS model.

B. Dynamics

The dynamics of the controlled SIS model can be derived following the same procedure used in Section III. In fact, despite being time-varying, the activity rate in (26) depends on t only through the state $x_i(t)$. Hence, all the dynamics involved in the epidemic process (contagion, recovery, and network formation) are independent Poisson processes, whose rate is constant given the state $\boldsymbol{x}$, yielding a homogeneous Markov chain, whose rates are computed in the following.

Proposition 6. *The transition rates in* (4) *for the controlled SIS model when* $\boldsymbol{x}(t) = \boldsymbol{x}$ *are*

$$\begin{aligned} q_i^{01}(x) = &\lambda a_i \frac{m}{n-1}\sum\nolimits_{j\in\mathcal{V}} x_j + \lambda(1-u_2)\frac{m}{n-1}\sum\nolimits_{j\in\mathcal{V}} a_j x_j \\ &+\lambda(1-u_1)\frac{m(m-1)}{(n-1)(n-2)}\sum_{j\in\mathcal{V}} x_j \sum_{\ell\in\mathcal{V}\setminus\{i,j\}} a_\ell \\ &-\lambda u_2(1-u_1)\frac{m(m-1)}{(n-1)(n-2)}\sum_{j\in\mathcal{V}} x_j \sum_{\ell\in\mathcal{V}\setminus\{i,j\}} a_\ell x_\ell, \end{aligned} \tag{27}$$

and $q_i^{10}(x) = \mu$.

Proof. The proof is reported in Appendix B □

Also for the controlled SIS model, the mean-field approach based on the study of the mean dynamics $y_i(t)$ can be followed, for which we can approximate the epidemic prevalence as $I(t) \approx z_1$, using (8). The ODEs that govern the evolution of the mean dynamics are derived in a similar fashion, obtaining the following result.

Proposition 7. *The mean-field dynamics of the controlled SIS model is the solution of the system of ODEs, for* $i \in \mathcal{V}$*:*

$$\begin{aligned} \dot{y}_i = (1-y_i)\lambda m \Bigg[&\frac{a_i}{n-1}\sum_{j\in\mathcal{V}} y_j + \frac{1-u_2}{n-1}\sum_{j\in\mathcal{V}} a_j y_j \\ &+\frac{(m-1)(1-u_1)}{(n-1)(n-2)}\sum_{j\in\mathcal{V}} y_j \sum_{\ell\in\mathcal{V}\setminus\{i,j\}} a_\ell \\ &-\frac{u_2(1-u_1)(m-1)}{(n-1)(n-2)}\sum_{j\in\mathcal{V}} y_j \sum_{\ell\in\mathcal{V}\setminus\{i,j\}} a_\ell y_\ell \Bigg] - \mu y_i. \end{aligned} \tag{28}$$

Proof. The proof is similar to the one of Proposition 3, using (27) instead of (5a), and details are thus omitted. □

It is worth noticing that the mean-field equations for the controlled SIS model reduces to the one of the uncontrolled SIS model computed in Proposition 3, when $u_1 = 1-\theta$ and $u_2 = 0$. The presence of the two control actions, introduces two multiplicative terms that linearly reduce the second and third contribution to the contagion mechanism. Interestingly, besides these two linear terms, the presence of the control action further introduces a fourth and negative contribution to contagion, which depends on the two control inputs in a bilinear fashion, making the impact of the two control actions nontrivial to be assessed. In the following, we will use again the mean-field theory employed for the uncontrolled SIS model to investigate the effectiveness of the two control actions and designing an optimal control policy to eradicate the disease.

VI. Results for the Controlled SIS Model

A. Epidemic threshold

It is straightforward to prove that Propositions 4 and 5 hold true also for the controlled SIS dynamics. Hence, it is appropriate to investigate how the two control actions impact the epidemic threshold in (12).

Theorem 2. *For large networks* ($n \to \infty$)*, the epidemic threshold for the controlled SIS dynamics in* (28) *is*

$$\sigma_c(u_1,u_2) := \frac{2}{m\alpha_1[m+1-u_1(m-1)-u_2+\sqrt{\Delta}]}, \tag{29}$$

with

$$\Delta = (m+1-(m-1)u_1-u_2)^2 + 4(1-u_2)(c_v^2-1). \tag{30}$$

If $\frac{\lambda}{\mu} < \sigma_c$*, then all trajectories converge to the DFE. If* $\frac{\lambda}{\mu} > \sigma_c$*, then all trajectories with initial conditions different from the DFE converge to an EE.*

Proof. We follow the same arguments used in the proof of Theorem 1. However, the presence of a fourth term in (28) complicates the computations. First, similar to (15), in the limit $n \to \infty$, we compute

$$\begin{aligned} \dot{y}_i = (1-y_i)\lambda m \Big[&a_i z_1 + (1-u_2)z_2 + (m-1)(1-u_1)\alpha_1 z_1 \\ &-u_2(1-u_1)(m-1)z_1 z_2 \Big] - \mu y_i, \end{aligned} \tag{31}$$

from which we derive the dynamics of the macroscopic variables z_1 and z_2 in (8) and (13), as

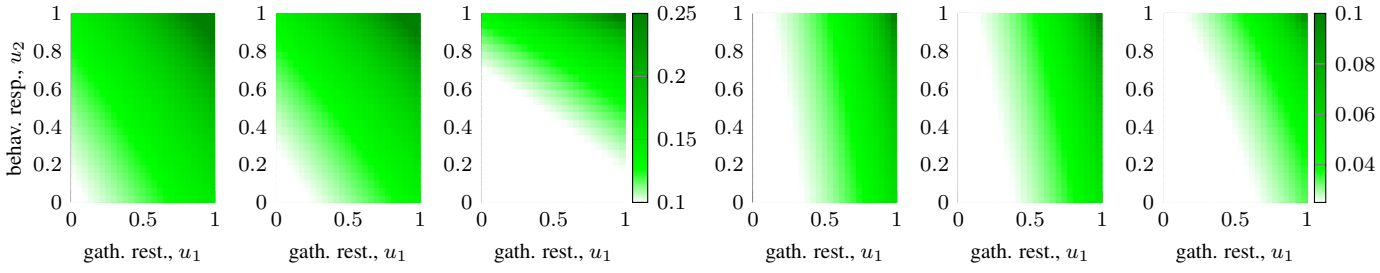
$$\begin{aligned} \dot{z}_1 = \lambda m \Big[&\alpha_1 z_1 - z_1 z_2 + z_2(1-z_1)(1-u_2) \\ &+(1-u_1)(m-1)\alpha_1 z_1(1-z_1) \\ &-u_2(1-u_1)(m-1)z_1 z_2(1-z_1) \Big] - \mu z_1, \end{aligned} \tag{32a}$$

and

$$\begin{aligned} \dot{z}_2 = \lambda m \Big[&\alpha_2 z_1 - z_1 \frac{1}{n}\sum a_i^2 y_i + (1-u_2)z_2(\alpha_1 - z_2) \\ &+(1-u_1)(m-1)\alpha_1 z_1(\alpha_1 - z_2) \\ &-u_2(1-u_1)(m-1)z_1 z_2(\alpha_1 - z_2) \Big] - \mu z_2. \end{aligned} \tag{32b}$$

By linearizing these two equations about the DFE (i.e., the origin), we obtain the following autonomous system:

$$\begin{aligned} \dot{z}_1 = &-\mu z_1 + \lambda m(m - m u_1 + u_1)\alpha_1 z_1 + \lambda m(1-u_2)z_2 \\ \dot{z}_2 = &-\mu z_2 + \lambda m((1-u_1)(m-1)\alpha_1^2 + \alpha_2)z_1 \\ &+\lambda m(1-u_2)\alpha_1 z_2, \end{aligned} \tag{33}$$



(a) $m = 3$, $c_v = 1$ (b) $m = 3$, $c_v = 1.5$ (c) $m = 3$, $c_v = 6$ (d) $m = 8$, $c_v = 1$ (e) $m = 8$, $c_v = 1.5$ (f) $m = 8$, $c_v = 6$

Fig. 4: Threshold from (29) as a function of the two control inputs, u_1 and u_2, for different orders of higher-order interactions m and coefficients of variation c_v (specified in the corresponding subcaption). The darker is the shade of green, the easier is to eradicate the disease.

whose Jacobian evaluated at the DFE is equal to

$$\begin{bmatrix} \lambda m(m - mu_1 + u_1)\alpha_1 - \mu & \lambda m(1 - u_2) \\ \lambda m((1 - u_1)(m - 1)\alpha_1^2 + \alpha_2) & \lambda m(1 - u_2)\alpha_1 - \mu \end{bmatrix}, \tag{34}$$

with eigenvalues $\xi_{1,2}$ that satisfy (after posing $\zeta = \xi + \mu$) the equation

$$\zeta^2 - \lambda m(m+1-u_1(m-1)-u_2)\alpha_1\zeta - \lambda^2 m^2(1-u_2)(\alpha_2-\alpha_1^2), \tag{35}$$

from which we conclude that the largest eigenvalue is negative iff $\lambda/\mu < \sigma_c$ from (29), yielding the claim. □

Remark 3. *In the absence of behavioral response, the threshold reduces to the one in Theorem 1. In the absence of gathering restrictions, the threshold reduces to the one of an SIS model with behavioral response on higher-order ADNs [21].*

B. Optimizing the control policy

A first, intuitive observation from the expression of the threshold in (29) is that control is always beneficial in increasing the threshold. In fact, in the denominator of σ_c, both u_1 and u_2 always appear with negative sign. Hence, increasing any of the control action would lead to an increase of the epidemic threshold, making the disease easier to be eradicated. However, how to assess the effectiveness of the different control actions is nontrivial, due to the intricate expression of the threshold.

For homogeneous networks, we can provide a clearer characterization of the effect of the control actions on the epidemic process, by simplifying the epidemic threshold as detailed in the following.

Corollary 2. *For large networks ($n \to \infty$), the epidemic threshold for the controlled SIS dynamics in* (28) *under Assumption 1 is*

$$\bar{\sigma}_c = \frac{1}{m\alpha_1(m + 1 - u_1(m - 1) - u_2)}. \tag{36}$$

Remark 4. *From the expression in* (36)*, we can perform a sensitivity analysis. Specifically, we can compute the derivative of the denominator of* (36)*, observing that*

$$\frac{\partial}{\partial u_1}[m\alpha_1(m+1-u_1(m-1)-u_2)] = -m(m-1)\alpha_1, \tag{37a}$$

and

$$\frac{\partial}{\partial u_2}[m\alpha_1(m + 1 - u_1(m - 1) - u_2)] = -m\alpha_1. \tag{37b}$$

From a comparison between the two expressions, we conclude that for any $m > 2$, $\frac{\partial}{\partial u_1}\bar{\sigma}_c(u_1, u_2) > \frac{\partial}{\partial u_2}\bar{\sigma}_c(u_1, u_2)$. Hence, it is always more effective, in homogeneous networks, to restrict gatherings (i.e., to exert control action u_1), rather than to enforce infected individuals to reduce their social activity. This could be due to the fact that, in homogeneous networks, the absence of highly socially active individuals may naturally reduce the impact of superspreader individuals, without the need of enforcing their isolation, thereby making more effective those policies that reduce superspreading events where multiple individuals may interact.

In the presence of heterogeneity, however, a further negative term that depends on u_2 emerges at the denominator of (29), rendering the determination of the preferred action less apparent. Although an approach similar to the one used in Remark 4 can be adopted, the complexity of the expression makes the analytical comparison of the two derivatives nontrivial. However, the closed-form expression for the threshold allows us to assess the effectiveness of the combination of the two control policies by evaluating (29) numerically as a function of the two control inputs.

Our results, reported in Fig. 4, depict a nontrivial scenario. On the one hand, for low levels of heterogeneity, the analytical predictions for homogeneous networks in Remark 4 are still valid, suggesting that the the results obtained for homogeneous networks are good approximations for mildly heterogeneous networks (compare,.e.g., Figs. 4a and 4b). Briefly, for moderate levels of heterogeneity it is more advantageous to invest in restricting gatherings (i.e., in action u_1). This difference is marginal for small values of m: when $m = 3$, setting $u_1 = 0.5$ would increase the threshold by 20% with respect to the uncontrolled scenario, compared to a 18% improvement when controlling with $u_2 = 0.5$ (Fig. 4b), but it becomes apparent as m increases. This can be seen, for example, in Fig. 4e, where the first control action leads to an improvement of 167%, outperforming the poor 8% achieved with the second action. On the other hand, a different scenario emerges when dealing with highly heterogeneous networks. In fact, from Fig. 4c, we observe that promoting a reactive response is more effective than the restriction of gatherings.: Controlling with $u_2 = 0.5$ yields a 26% improvement in the threshold, outperforming the 14% improvement achieved with $u_1 = 0.5$.

In summary, in real-world systems, which are often het-

erogeneous, the effectiveness of the two control actions is nontrivial and highly dependent on the characteristics of the population. This underscores the significance of deriving an analytical expression for the epidemic threshold, which serves as a tool to quantitatively evaluate the efficacy of the two control strategies. It also facilitates their optimal combination to enhance the epidemic threshold, potentially subject to budgetary limitations, thereby formulating an optimization problem in the following manner:

$$\begin{array}{ll} \text{minimize} & f(u_1,u_2) \\ \text{s.t.} & c(u_1,u_2)\le B \\ & u_1\in[0,1],\ u_2\in[0,1], \end{array} \tag{38}$$

where

$$f(u_1,u_2)=m+1-(m-1)u_1-u_2 \\ +\sqrt{\big(m+1-(m-1)u_1-u_2\big)^2+4(1-u_2)(c_v^2-1)} \tag{39}$$

is the denominator of the epidemic threshold in (29), $c(u_1,u_2):[0,1]\times[0,1]\to\mathbb{R}_{\ge 0}$ is a monotonically increasing cost function associated with the implementation of the control actions, and $B\in\mathbb{R}_{\ge 0}$ is the total budget available. At first sights, the nonconvexity of the objective function may hinder its treatment. However, we can observe the following.

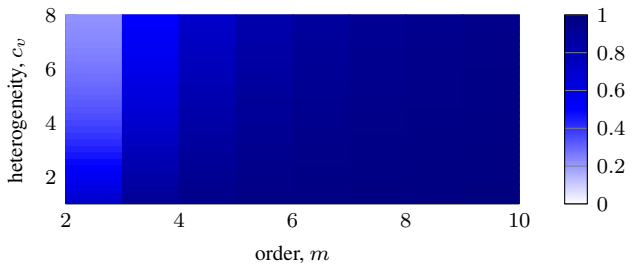
Proposition 8. *The solution of* (38) *coincides with the solution of a one-dimensional minimization problem with objective function* $f(u_1,\phi(u_1))$*, with* $\phi(u_1)=\min\{\max\{u_2\in[0,1]: c(u_1,u_2)\le B\},1\}$*,* $u_1\in[0,\bar{u}_1]$*, and* $\bar{u}_1=\min\{\max\{u_1\in[0,1]: c(u_1,0)\le B\},1\}$.

Proof. The statement is equivalent to saying that the solution of (38) lies on the boundary of the domain. We prove this by contradiction. Assume that (u_1^*,u_2^*) is the solution of (38) and it is not on the boundary. Hence, there exists $\varepsilon>0$ such that $c(u_1^*,u_2^*+\varepsilon)\le B$ and $u_2^*+\varepsilon\le 1$. Since the objective function f is monotonically decreasing in both u_1 and u_2, we get $f(u_1^*,u_2^*+\varepsilon)<f(u_1^*,u_2^*+\varepsilon)$, which leads to a contradiction, yielding the claim. □

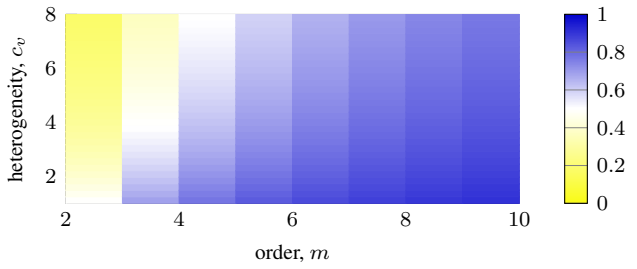
For instance, if the cost function is quadratic, i.e., $c(u_1,u_2)=c_1u_1^2+c_2u_2^2$, which captures the diminishing return often present in real-world intervention policies, Proposition 8 guarantees that the solution of (38) can be computed by solving the one-dimensional minimization problem with objective function $f(u_1,\min\{\sqrt{\frac{B-c_1u_1^2}{c_2}},1\})$. The numerical solution of this problem, when $c_1=c_2=1$ is reported in Fig. 5, suggesting that the optimal control policy entails a nontrivial combination of gathering restrictions and behavioral response, with the parameters c_v and m shaping the optimal mixing in a way consistent with our observations from Fig. 4 —u_1 is dominant for m large, u_2 is dominant for c_v large— but with both elementary control actions (almost) always present.

VII. Conclusion

We studied the spread of an epidemic disease on realistic temporal networks, in which both pairwise and higher-order interactions coexist in variable proportion, the latter capturing potential superspreading events. Building on the paradigm



(a) Optimal control action u_1



(b) Optimal mixing (relative magnitude of u_1)

Fig. 5: Optimal control policy computed by solving (38) for a quadratic control costs $c(u_1,u_2)=u_1^2+u_2^2$ with budget $B=1$ and different order of interactions m and heterogeneity c_v. In (a), the intensity of blue represents the optimal value of control action u_1. In (b), the color represents the relative magnitude of u_1 with respect to u_2 in the optimal control policy. The darker is the blue, the larger is the relative value of u_1 with respect to u_2; vice versa for for the intensity of yellow.

of activity-driven networks and employing a mean-field approach, we derived a set of ordinary differential equations that describe the mean dynamics of the epidemic process, whose analysis allowed us to elucidate the impact of higher-order interactions on shaping the spread of an epidemic outbreak.

Besides the model formulation, our main contribution was threefold. First, we derived the epidemic threshold, providing analytical insights into how the presence of these interactions shapes the outcome of the epidemic outbreak. Second, we incorporated two control actions in the system; namely, restricting gatherings and promoting a behavioral response and we have established how the presence of these two control actions favor the convergence to the disease-free equilibrium. Third, building on these theoretical results, we derived a quantitative framework to assess the effectiveness of these control actions and design control policies by optimally mixing them. Our results have not only provided evidence that large gatherings can play a critical role in favoring contagion, supporting their ban during epidemic outbreaks, but have also offered model-informed tools to help assist decision-makers in optimally designing interventions during an epidemic outbreak.

The approach presented in this paper is not exempt from limitations. First, our results focus on the problem of eradicating a disease by implementing control actions that increase the epidemic threshold. In some circumstances, however, it is crucial to assess the effect different control actions, e.g., to mitigate endemic diseases that cannot be fully eradicated [37], [38]. To extend our tools to deal with such scenarios, a theoretical analysis of the behavior of the system above the epidemic threshold is needed, with a characterization of the

endemic equilibria. Second, this paper is concerned with the analysis of the SIS model. Many real-world epidemic diseases, however, are characterized by (permanent or waning) immunity after recovery. Our successful analytical treatment of the SIS model provides good prospects for the analysis of more complex models that account for such herd immunity (e.g., SIR-like models used for COVID-19 [35]). This extension is key to broaden the model's relevance to a wider range of epidemic scenarios. Third, the behavioral responses of infected individuals are often not instantaneous but exhibit a certain delay effect. While the current model does not capture this phenomenon, its impact can be studied by introducing a time delay (see.,e.g., [53]) or by using more complex and realistic models for human behavior (e.g., using game-theory [34]).

References

[1] E. Valdano, L. Ferreri, C. Poletto, and V. Colizza, "Analytical computation of the epidemic threshold on temporal networks," *Phys. Rev. X*, vol. 5, p. 021005, 2015.

[2] P. Holme, "Temporal network structures controlling disease spreading," *Phys. Rev. E*, vol. 94, no. 2, 2016.

[3] M. Ogura, V. M. Preciado, and N. Masuda, "Optimal containment of epidemics over temporal activity-driven networks," *SIAM J. Appl. Math.*, vol. 79, no. 3, pp. 986–1006, 2019.

[4] R. Humphries, K. Mulchrone, J. Tratalos, S. J. More, and P. Hövel, "A systematic framework of modelling epidemics on temporal networks," *Appl. Netw. Sci.*, vol. 6, no. 1, 2021.

[5] L. Zino and M. Cao, "Analysis, prediction, and control of epidemics: A survey from scalar to dynamic network models," *IEEE Circuits Syst. Mag.*, vol. 21, no. 4, pp. 4–23, 2021.

[6] C. Li, Y. Zhang, and X. Li, "Epidemic threshold in temporal multiplex networks with individual layer preference," *IEEE Trans. Netw. Sci. Eng.*, vol. 8, no. 1, pp. 814–824, 2021.

[7] Y. Liu, R. M. Eggo, and A. J. Kucharski, "Secondary attack rate and superspreading events for SARS-CoV-2," *Lancet*, vol. 395, no. 10227, p. e47, 2020.

[8] J. E. Lemieux *et al.*, "Phylogenetic analysis of SARS-CoV-2 in Boston highlights the impact of superspreading events," *Science*, vol. 371, no. 6529, 2021.

[9] P. R. Carlin, P. Minard, D. H. Simon, and C. Wing, "Effects of large gatherings on the COVID-19 epidemic: Evidence from professional and college sports," *Econ. Hum. Biol.*, vol. 43, p. 101033, 2021.

[10] B. C. Mweene, L. Muchaili, and S. K. Masenga, "The re-emergence of mpox: A global public health threat amplified by mass gatherings," *Mass Gather. Med.*, vol. 4, p. 100023, 2025.

[11] C. Bick, E. Gross, H. A. Harrington, and M. T. Schaub, "What are higher-order networks?" *SIAM Rev.*, vol. 65, no. 3, pp. 686–731, 2023.

[12] G. Bianconi, *Higher-Order Networks*. Cambridge, UK: Cambridge University Press, 2021.

[13] S. Boccaletti *et al.*, "The structure and dynamics of networks with higher order interactions," *Phys. Rep.*, vol. 1018, pp. 1–64, 2023.

[14] W. Wang, Y. Nie, W. Li, T. Lin, M.-S. Shang, S. Su, Y. Tang, Y.-C. Zhang, and G.-Q. Sun, "Epidemic spreading on higher-order networks," *Phys. Rep.*, vol. 1056, p. 1–70, 2024.

[15] G. Petri and A. Barrat, "Simplicial activity driven model," *Phys. Rev. Lett.*, vol. 121, p. 228301, 2018.

[16] S. Huang, Y.-H. Xu, M.-Y. Li, and M.-B. Hu, "Effect of behavioral changes on epidemic spreading in coupled simplicial activity driven networks," *J. Stat. Mech*, vol. 2023, no. 12, p. 123405, 2023.

[17] S. Zhang, D. Zhao, C. Xia, and J. Tanimoto, "Impact of simplicial complexes on epidemic spreading in partially mapping activity-driven multiplex networks," *Chaos*, vol. 33, no. 6, 2023.

[18] P. Cisneros-Velarde and F. Bullo, "Multigroup SIS epidemics with simplicial and higher order interactions," *IEEE Trans. Control Netw. Syst.*, vol. 9, no. 2, pp. 695–705, 2022.

[19] J. Fan, Q. Yin, C. Xia, and M. Perc, "Epidemics on multilayer simplicial complexes," *Proc. R. Soc. A*, vol. 478, no. 2261, 2022.

[20] S. Cui, F. Liu, L. Liang, H. Jardón-Kojakhmetov, and M. Cao, "An SIS diffusion process with direct and indirect spreading on a hypergraph," *Automatica*, vol. 177, p. 112319, 2025.

[21] L. Zino and A. Rizzo, "On a susceptible-infected-susceptible epidemic model with reactive behavioral response on higher-order temporal networks," in *IEEE 63rd Conf. Decis. Control*, 2024, pp. 3912–3917.

[22] Q. Zhu, "Event-triggered sampling problem for exponential stability of stochastic nonlinear delay systems driven by Lévy processes," *IEEE Trans. Autom. Control*, vol. 70, no. 2, pp. 1176–1183, 2025.

[23] B. Wang and Q. Zhu, "The stabilization problem for a class of discrete-time semi-markov jump singular systems," *Automatica*, vol. 171, p. 111960, Jan. 2025.

[24] K. Drakopoulos, A. Ozdaglar, and J. N. Tsitsiklis, "An efficient curing policy for epidemics on graphs," *IEEE Trans. Netw. Sci. Eng.*, vol. 1, pp. 67–75, 2014.

[25] C. Nowzari, V. M. Preciado, and G. J. Pappas, "Optimal resource allocation for control of networked epidemic models," *IEEE Control Netw. Syst.*, vol. 4, no. 2, pp. 159–169, 2017.

[26] V. M. Preciado, M. Zargham, C. Enyioha, A. Jadbabaie, and G. J. Pappas, "Optimal Resource Allocation for Network Protection Against Spreading Processes," *IEEE Trans. Control Netw. Syst.*, vol. 1, no. 1, pp. 99–108, 2014.

[27] V. L. J. Somers and I. R. Manchester, "Sparse Resource Allocation for Control of Spreading Processes via Convex Optimization," *IEEE Control Syst. Lett.*, vol. 5, no. 2, pp. 547–552, 2021.

[28] L. Walsh, M. Ye, B. D. Anderson, and Z. Sun, "Decentralised adaptive-gain control for eliminating epidemic spreading on networks," *Automatica*, vol. 174, p. 112143, 2025.

[29] A. R. Hota and S. Sundaram, "Game-theoretic vaccination against networked sis epidemics and impacts of human decision-making," *IEEE Control Netw. Syst.*, vol. 6, no. 4, p. 1461–1472, Dec. 2019.

[30] M. Xia, L. Böttcher, and T. Chou, "Controlling epidemics through optimal allocation of test kits and vaccine doses across networks," *IEEE Tran. Netw. Sci. Eng.*, vol. 9, no. 3, pp. 1422–1436, 2022.

[31] F. Galante, C. Ravazzi, M. Garetto, and E. Leonardi, "Planning interventions in a controlled pandemic: The COVID-19 case," *IEEE Tran. Netw. Sci. Eng.*, vol. 11, no. 2, p. 2314–2331, 2024.

[32] M. Alutto, G. Como, and F. Fagnani, "On SIR epidemic models with feedback-controlled interactions and network effects," in *Proc. 60th IEEE Conf. Decis. Control*, 2021, pp. 5562–5567.

[33] L. Zino, A. Rizzo, and M. Porfiri, "On assessing control actions for epidemic models on temporal networks," *IEEE Control Syst. Lett.*, vol. 4, no. 4, pp. 797–802, 2020.

[34] N. C. Martins, J. Certório, and R. J. La, "Epidemic population games and evolutionary dynamics," *Automatica*, vol. 153, p. 111016, 2023.

[35] G. Giordano *et al.*, "Modelling the COVID-19 epidemic and implementation of population-wide interventions in Italy," *Nat. Med.*, vol. 26, pp. 855–860, 2020.

[36] F. Della Rossa *et al.*, "A network model of Italy shows that intermittent regional strategies can alleviate the COVID-19 epidemic," *Nat. Comm.*, vol. 11, no. 1, p. 5106, 2020.

[37] R. Carli, G. Cavone, N. Epicoco, P. Scarabaggio, and M. Dotoli, "Model predictive control to mitigate the COVID-19 outbreak in a multi-region scenario," *Annu. Rev. Control*, vol. 50, pp. 373–393, 2020.

[38] J. Köhler, L. Schwenkel, A. Koch, J. Berberich, P. Pauli, and F. Allgöwer, "Robust and optimal predictive control of the COVID-19 outbreak," *Annu. Rev. Control*, vol. 51, p. 525–539, 2021.

[39] A. R. Hota, J. Godbole, and P. E. Paré, "A closed-loop framework for inference, prediction, and control of SIR epidemics on networks," *IEEE Tran. Netw. Sci. Eng.*, vol. 8, no. 3, pp. 2262–2278, 2021.

[40] L. Zino, A. Rizzo, and M. Porfiri, "Continuous-time discrete-distribution theory for activity-driven networks," *Phys. Rev. Lett.*, vol. 117, 2016.

[41] J. A. Yorke, H. W. Hethcote, and A. Nold, "Dynamics and control of the transmission of gonorrhea," *Sex. Transm. Dis.*, vol. 5, no. 2, pp. 51–55, 1978.

[42] P. V. Mieghem, J. Omic, and R. Kooij, "Virus spread in networks," *IEEE/ACM Trans. Netw.*, vol. 17, no. 1, pp. 1–14, Feb 2009.

[43] T. Hale *et al.*, "A global panel database of pandemic policies (Oxford COVID-19 government response tracker)," *Nat. Hum. Behav.*, vol. 5, no. 4, p. 529–538, 2021.

[44] A. Rizzo, M. Frasca, and M. Porfiri, "Effect of individual behavior on epidemic spreading in activity driven networks," *Phys. Rev. E*, vol. 90, 2014.

[45] N. T. J. Bailey, *The Elements of Stochastic Processes with Applications to the Natural Sciences*. Hoboken NJ, US: Wiley, 1990.

[46] J. Mossong *et al.*, "Social contacts and mixing patterns relevant to the spread of infectious diseases," *PLoS Med.*, vol. 5, no. 3, p. e74, 2008.

[47] F. Blanchini, "Set invariance in control," *Automatica*, vol. 35, no. 11, pp. 1747–1767, 1999.

[48] H. L. Smith, *Monotone Dynamical Systems: An Introduction to the Theory of Competitive and Cooperative Systems*. Providence RI, US: American Mathematical Society, 2008, no. 41.
[49] N. Perra, B. Gonçalves, R. Pastor-Satorras, and A. Vespignani, "Activity driven modeling of time varying networks," *Sci. Rep.*, vol. 2, 2012.
[50] Centers for Disease Control and Prevention, "2022-2023 mpox outbreak global map," https://www.cdc.gov/poxvirus/mpox/response/2022/world-map.html.
[51] P. E. M. Fine, Z. Jezek, B. Grab, and H. Dixon, "The transmission potential of monkeypox virus in human populations," *Int. J. Epidem.*, vol. 17, no. 3, p. 643–650, 1988.
[52] H. W. Chung *et al.*, "Effects of government policies on the spread of COVID-19 worldwide," *Sci. Rep.*, vol. 11, no. 1, 2021.
[53] F. Liu, L. Shi, J. Shao, and Q. Liu, "On a discrete-time networked epidemic model with time-varying heterogeneous delays," *IEEE Control Syst. Lett.*, vol. 8, p. 2289–2294, 2024.

APPENDIX

A. Proof of Proposition 2

The proof follows [21, Proposition 1]. For the sake of completeness, we briefly report it, highlighting the key differences.

The rate $q_i^{01}(x)$ is associated with contagion, which occurs if i has a contact with an infected individual and the disease is transmitted. Since the latter occurs each contact independent of the others, we compute separately the rate at which a generic individual j transmits the disease to i, and then we sum them, according to Proposition 1.i).

Individual j transmits the disease to i if one of the following chains of events occurs: i) i activates, j is one of the m nodes selected, j is infected, and the disease is transmitted; ii) j activates, j is infected, i is one of the m nodes selected, and the disease is transmitted; iii) an individual $\ell \in \mathcal{V} \setminus \{i,j\}$ activates, both i and j are among the m nodes selected by ℓ, ℓ has a higher-order interaction, j is infected, and the disease is transmitted. Whether the node has a pairwise or a higher-order interaction affects only the third chain. In fact, if ℓ decides to engage in pairwise interactions, then no interaction between i and j is established, so no contagion can occur at time t.

For each one of these chains, we use Proposition 1.ii) to compute the corresponding rate. Chain i) is triggered by the Poisson clock that regulates the activation of i, split by a sequence of three Bernoulli random variables associated with three events: a) node j is selected, b) node j is infected, and c) the disease is transmitted. Since all these events are independent, according to Proposition 1.ii), we compute the rate associated with this chain, obtaining $\lambda a_i \frac{m}{n-1} x_j$, where $x_j \in \{0,1\}$ is an indicator function that annihilates the rate when j is not infected. Chain ii) is studied similarly (see [21] for more details), obtaining $\lambda a_j \frac{m}{n-1} x_j$.

For chain iii), we observe that the activation of each individual is independent of the others. Hence, following the same arguments used above, the rate of chain iii) is equal to the sum over all $\ell \in \mathcal{V} \setminus \{i,j\}$ of the product between the individual activity rate a_ℓ, the probability of selecting both i and j in a random m-uple (which is equal to $\frac{m(m-1)}{(n-1)(n-2)}$), the probability of engaging in a higher-order interaction (which is θ) the infection probability λ, and the indicator x_j, yielding

$$\sum\nolimits_{\ell \in \mathcal{V}\setminus\{i,j\}} \lambda\theta \frac{m(m-1)}{(n-1)(n-2)} a_\ell x_j, \tag{40}$$

which differ from the corresponding term in [21] for the presence of the factor θ. The total rate at which j transmits the disease to i is computed by summing the three contributions, and then summing then over all $j \in \mathcal{V}$, obtaining (5a). Finally, recovery is spontaneously triggered by a Poisson process with rate μ, yielding (5b). □

B. Proof of Proposition 6

The rates are obtained following the arguments used in the proof of Proposition 2, replacing $\theta = 1 - u_1$, with a key difference. In fact, if j is infected, then their activity rate is reduced to $(1 - u_2)a_j$. This should be considered when deriving the rates associated with the three chains of events. In particular, in chain i), the interaction is initiated by a susceptible individual, so $\hat{a}_i = a_i$, yielding no changes to the rate. For chain ii), instead, the interaction is initiated by an infected individual j, with $\hat{a}_j = (1 - u_2)a_j$, which re-scales the contribution by a multiplicative constant $(1 - u_2)$. For chain iii), we need to split the contribution in two distinct terms, depending on the health state of ℓ. Then, re-arranging the terms, the rate associated with the third chain is equal to

$$\sum_{\ell \in \mathcal{V}\setminus\{i,j\}} \lambda(1-u_1)\frac{m(m-1)}{(n-1)(n-2)} a_\ell x_j \big(1 - u_2 x_\ell\big). \tag{41}$$

Finally, (29) is obtained by summing the three rates and then summing over all $j \in \mathcal{V}$. □



Lorenzo Zino is an Assistant Professor with the Department of Electronics and Telecommunications, Politecnico di Torino, Italy, since 2022. He received BS (2012), MS (summa cum laude, 2014), and PhD (with honors, 2018) in Applied Mathematics from Politecnico di Torino. He held Research Fellowships at Politecnico di Torino, University of Groningen, and New York University. His research interests include modeling, analysis, and control of dynamics over networks, applied probability, and game theory; and he has co-authored more than 90 international scientific publications, including more than 50 journal papers. In 2024, he received the Best Young Author Journal Paper Award from the IEEE CSS Italy Chapter. He is Associate Editor of the *Journal of Computational Science*, the *International Journal of Control*, member of the Editorial Board of *Scientific Reports*, and of the Conference Editorial Board for IEEE CSS and EUCA.



Alessandro Rizzo is an Associate Professor at the Department of Electronics and Telecommunications, Politecnico di Torino, Italy, where he coordinates the Complex Systems Laboratory. He received his Laurea degree in Computer Engineering, summa cum laude, and his PhD in Automation and Electronics Engineering from the University of Catania, in 1996 and 2000, respectively. Dr. Rizzo's previous affiliations include JET Joint Undertaking, ST Microelectronics, the University of Messina, Politecnico di Bari, and New York University. His research interests span complex networks and systems, robotics, and the modeling and control of nonlinear systems. He has authored two books, holds two international patents, and has published over 200 papers in peer-reviewed international journals and conference proceedings. A Distinguished Lecturer for the IEEE Nuclear and Plasma Sciences Society, he received the Best Application Paper Award at the 2002 IFAC World Congress, as well as two Amazon Research Awards in Robotics (2019, 2021).